Dalton Transactions

RSC Publishing

PAPER

View Article Online
View Journal | View Issue

Cite this: *Dalton Trans.*, 2013, **42**, 12495

Ligand dependent self-assembly of hydroxido-bridged dicopper units templated by sodium ion†

Avijit Sarkar,[a] Alok Ranjan Paital,[a] Rais Ahmad Khan,[b] Farukh Arjmand,[b] Valerio Bertolasi,[c] Corine Mathonière,[d,e] Rodolphe Clérac[f,g] and Debashis Ray*[a]

Received 26th April 2013,
Accepted 5th June 2013

DOI: 10.1039/c3dt51095f

www.rsc.org/dalton

Crown-ether like interaction of two neutral $[Cu_2(\mu\text{-}OH)(\mu\text{-}L^1)]$ (H_3L^1 = 2-(2′-hydroxyphenyl)-1,3-bis[4-(2-hydroxyphenyl)-3-azabut-3-enyl]-1,3-imidazolidine) fragments, around a central Na^+ cation as self-assembly template, led to the formation of $[Na\{Cu_2(\mu\text{-}OH)(\mu\text{-}L^1)\}_2]ClO_4$ (**1**). Di-*tert*-butyl group substituted H_3L^2 {2-(3,5-di-*tert*-butyl-2-hydroxyphenyl)-1,3-bis[4-(3,5-di-*tert*-butyl-2-hydroxyphenyl)-3-azabut-3-enyl]-1,3-imidazolidine} conversely yields only $[Cu_2(\mu\text{-}OH)(\mu\text{-}L^2)]\cdot 1.5H_2O$ (**2**), by discarding aggregation around the Na^+ ion. The crown-ether type aggregate **1** exhibits ferromagnetic interactions within the double oxido-phenoxido $[Cu_2]$ fragments and weak antiferromagnetic interactions are mediated by the O···Na^+···O bridges. Complex **2** registers only weak antiferromagnetic interactions within the oxido-phenoxido bridged $[Cu_2]$ entity. UV-visible and emission titration spectroscopy establish the interaction of cationic complex **1** with calf thymus DNA in Tris buffer and it cleaves supercoiled pBR322 DNA from *in situ* generated ROS.

Introduction

Crown ethers are cyclic covalent compounds consisting of rings containing ether groups and have been known as size-specific cation-binding species for over 40 years.[1] The inorganic structural analogues of crown ethers, popularly known as metallacrowns, are coordination compounds formed from self-assembly of several metal ions and oximate based ligands.[2] Study of crown ethers and metallacrowns can greatly enrich our knowledge of host–guest chemistry as both of these are good host molecules. In many cases, the metal–organic cyclic frame does not exist without the incorporation of guest cation, which plays the role of a cation template.[3,4] For the construction of transition-metal based cage-like compounds with interesting structures and properties, the template reaction has been extensively used. It is worth noting that in most of the cases these systems would not have formed without this template approach.[5,6] Use of Na^+ or other similar cations as a template for the assembly of two dinuclear units requires, besides transition-metal ions such as Cu^{2+}, phenolate based ligands capable of both coordinating and bridging the Cu^{2+} ions and interacting with the templating cation. Anions such as Cl^-, N_3^-, HO^- or O^{2-} can instead interact through direct coordination with metal ions having at least one vacant coordination site and can function as coordinating nucleating groups for the newer metal–ligand assembly.[7–10] Thus synthetic coordination chemistry that facilitates controlled aggregation around these anions to generate polynuclear complexes is of great interest. Involvement of double hydroxido bridges for a tetranuclear Cu_4 assembly has been studied by us on a piperazine based ligand.[11] The role of the ligand structure, the fine-tuning of reaction conditions and the nature of the bases are crucial to generate water-derived HO^- and O^{2-} groups and to control the aggregation process. The Cu_2 complexes considered so far as models to study magnetic exchange interactions,[12–14] DNA binding and cleavage,[15] oxidation of catechols,[13,16,17] and act as hydrolytic agents for glycosides[18] can also be used as building motifs for the construction of newer tetra- and polynuclear assemblies.[19–22] In general, the assembly of two dinuclear units leads to four types of Cu_4 aggregates, namely tetrahedron, cubane, partial dicubane and stepped cubane.[9] We have shown that the O^{2-} anion can function as a nucleating group for $Cu_4(\mu_4\text{-}O)$ aggregate formation from the assembly of two Cu_2 units bound to different ligand systems.[23–25] While trying to isolate and study newer forms of

[a]*Department of Chemistry, Indian Institute of Technology, Kharagpur 721 302, India. E-mail: dray@chem.iitkgp.ernet.in; Fax: (+91) 3222-82252; Tel: (+91) 3222-283324*
[b]*Department of Chemistry, Aligarh Muslim University, Aligarh, UP-202002, India*
[c]*Dipartimento di Scienze Chimiche e Farmaceutiche, Centro di Strutturistica Diffrattometrica, Università di Ferrara, via Borsari 46, 44121 Ferrara, Italy*
[d]*CNRS, ICMCB, UPR 9048, F-33600 Pessac, France*
[e]*Univ. Bordeaux, ICMCB, UPR 9048, F-33600 Pessac, France*
[f]*CNRS, CRPP, UPR 8641, F-33600 Pessac, France*
[g]*Univ. Bordeaux, CRPP, UPR 8641, F-33600 Pessac, France*

†Electronic supplementary information (ESI) available: Scheme S1, Fig. S1–S4, synthesis and characterization of ligands H_3L^1 and H_3L^2. CCDC reference numbers 651162 and 840821 for **1** and **2**, respectively. For ESI and crystallographic data in CIF or other electronic format see DOI: 10.1039/c3dt51095f

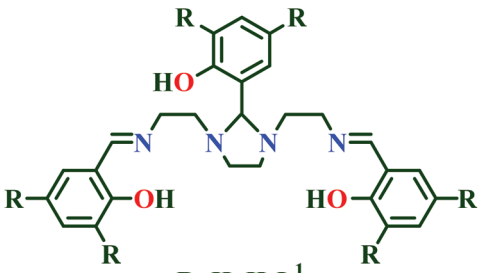

R=H, H_3L^1

R= tert-butyl, H_3L^2

Chart 1

such assemblies, we have been interested to explore the reactivity of the dinucleating heptadentate phenol based ligands H_3L^n {Chart 1: n = 1 for 2-(2′-hydroxyphenyl)-1,3-bis[4-(2-hydroxyphenyl)-3-azabutenyl]-3-enyl]-1,3-imidazolidine)[26] and n = 2 for 2-(3,5-di-*tert*-butyl-2-hydroxyphenyl)-1,3-bis[4-(3,5-di-*tert*-butyl-2-hydroxyphenyl)-3-azabutenyl]-1,3-imidazolidine)[27]} with Cu(II) ions.

In addition, Cu(II) complexes have been reported to serve as potential pharmacological agents and as potential anticancer and cancer-inhibiting agents.[28–32] Numerous examples of mixed-ligand Cu(II) complexes,[33–35] which strongly bind and cleave DNA, exhibit prominent anticancer activities and regulate apoptosis. Various studies demonstrated that multinuclear Cu(II) complexes can promote DNA cleavage significantly by selectively oxidizing deoxyribose or nucleobase moieties.[36] The copper centers in multinuclear complexes act synergistically to cleave DNA with higher efficiency or selectivity.[37,38] Therefore, nuclearity is considered as a crucial parameter for DNA cleavage.[39,40] Design of multinuclear copper complexes with suitable recognition elements in the ligand scaffold for binding and cleavage of DNA has drawn considerable attention in recent years.

Herein, two copper(II) complexes are reported: (i) $[Na\{Cu_2(\mu\text{-}OH)(\mu\text{-}L^1)\}_2]ClO_4$ (**1**), which contains a central Na^+ template bound to two *facial* O_3 halves from each tris-phenol based ligands, and (ii) $[Cu_2(\mu\text{-}OH)(\mu\text{-}L^2)]\cdot 1.5H_2O$ (**2**), obtained from the *tert*-butyl substituted analogue of the former ligand inhibiting aggregate formation around the cationic template. These complexes have been synthesized, isolated and characterized crystallographically. Their magnetic properties and interaction with DNA have been also examined.

Experimental section

Materials and physical methods

All the starting chemicals and solvents were analytically pure and used without further purification. 2-(2′-Hydroxyphenyl)-1,3-bis[4-(2-hydroxyphenyl)-3-azabut-3-enyl]-1,3-imidazolidine (H_3L^1)[27] and 2-(3,5-di-*tert*-butyl-2-hydroxyphenyl)-1,3-bis[4-(3,5-di-*tert*-butyl-2-hydroxyphenyl)-3-azabut-3-enyl]-1,3-imidazolidine) (H_3L^2)[28] were prepared as previously described. All other chemicals and solvents were reagent grade materials and were used as received without further purification. The elemental analyses (C, H, N) were performed with a Perkin-Elmer model 240C elemental analyzer. FTIR spectra were recorded on a Perkin-Elmer Spectrum RX1 spectrometer. The solution electrical conductivity and electronic spectra were obtained using a Unitech type U131C digital conductivity meter with a solute concentration of about 10^{-3} M and a Shimadzu UV 2450UV-vis spectrophotometer, respectively. For the DNA binding study, electronic spectra were recorded on a UV-1700 PharmaSpec UV-vis spectrophotometer (Shimadzu). Emission spectra were determined with a Hitachi F-2500 fluorescence spectrophotometer. Magnetic susceptibility measurements were obtained with the use of a Quantum Design SQUID magnetometer MPMS-XL. This magnetometer works between 1.8 and 400 K for dc applied fields ranging from −7 to 7 T. Measurements were performed on microcrystalline samples of 12.57 mg and 18.51 mg for **1** and **2**, respectively. The magnetic data are corrected for the sample holder and the diamagnetic contributions. Cleavage experiments were performed with the help of Axygen electrophoresis supported by Genei power supply with a potential range of 50–500 V, visualized and photographed by a Vilber-INFINITY Gel documentation system. DNA binding experiments that include absorption spectral studies, fluorescence studies and cleavage experiments conform to the standard methods[41–43] and practices previously adopted.[44,45] Standard error limits were estimated using all data points.

Caution! *Perchlorate salts are potentially explosive, only a small amount should be prepared and handled with proper care.*

Synthesis

H_3L^1 and H_3L^2 ligands. Two tris-phenol based ligands were prepared from the single-step Schiff-base condensation reactions of salicylaldehyde (5.89 mL, 15 mmol) and 3,5-di-*tert*-butyl-2-hydroxybenzaldehyde (11.91 g, 15 mmol) with triethylenetetramine (0.74 mL, 5 mmol) in MeOH (30 mL) for 2 h, as reported previously.[27,28]

$[Na\{Cu_2(\mu\text{-}OH)(\mu\text{-}L^1)\}_2]ClO_4$ (1). To a yellow dichloromethane solution (15 mL) of H_3L^1 (0.50 g, 1.09 mmol) a MeOH solution (10 mL) of NaOH (0.174 g, 4.36 mmol) was added dropwise followed by another MeOH solution (5 mL) of $Cu(ClO_4)_2\cdot 6H_2O$ (0.80 g, 2.18 mmol) with stirring at ambient temperature in air. The resulting green solution was stirred for 1 h during which no solid product separated. The green solution was then evaporated in air at ambient temperature and after about 6 h a green precipitate appeared. The deep green solid was isolated by filtration through a G4 glass frit, washed with water followed by ethanol and hexane and dried under *vacuo* over P_4O_{10}. Green plate-like single crystals suitable for X-ray analysis were obtained from an acetonitrile solution after 6 days. Yield: 0.54 g, 75%. Anal. Calc. for $C_{54}H_{56}N_8O_{12}NaClCu_4$ (1321.66 g mol^{-1}): C, 49.07; H, 4.27; N, 8.48. Found: C, 48.98; H, 4.35; N, 8.56%. Selected FTIR bands: (KBr, cm^{-1}, vs = very strong, s = strong, m = medium, w = weak): 3447 (vs) 2371 (vs), 1635 (vs), 1458(s), 1313 (s), 1049 (m), 775 (m), 625 (w). Molar conductance, Λ_M (DMF solution): 130 Ω^{-1} cm^2 mol^{-1}. UV-vis

spectra [λ_{max}/nm (ε/L mol^{-1} cm^{-1})]: (CH_3CN solution) 600 (410), 397 (24 160), 358 (26 460).

[Cu_2(μ-OH)(μ-L^2)]·1.5H_2O (2). To a MeOH solution (20 mL) of H_3L^2 (0.79 g, 1 mmol), another MeOH solution (5 mL) of $Cu(ClO_4)_2·6H_2O$ (0.74 g, 2 mmol) was added dropwise with magnetic stirring during 15 min. After 30 min, a MeOH solution (5 mL) of NaOH (0.16 g, 4 mmol) was added slowly to the previous solution during 10 min. The reaction mixture was then stirred for another 30 min. A deep green solid was separated from the resulting green solution on solvent evaporation in air. The product was collected by filtration through a glass frit and washed thoroughly with water. The compound was finally dried *in vacuo* over P_4O_{10}. Green single crystals suitable for X-ray analysis were obtained from CH_3OH after one week. Yield: 0.54 g, 75%. Anal. Calc. for $C_{51}H_{76}Cu_2N_4O_4·1.5H_2O$ (963.26 g mol^{-1}): C, 63.59; H, 8.27; N, 5.82. Found: C, 63.32; H, 8.17; N, 5.88%. FTIR (KBr, cm^{-1}): 3448(br), 2371(m), 1629(s), 1459(s), 1167(s). Molar conductance, Λ_M (CH_3CN solution) 3 Ω^{-1} cm^2 mol^{-1}. UV-vis spectra (CH_3CN), [λ_{max}/nm (ε/L mol^{-1} cm^{-1})]: 660 (144), 392 (3285), 253 (15 281), 234 (16 827).

Results and discussion

Synthesis and characterization

The ligands H_3L^1 and H_3L^2 were prepared (Scheme S1 in ESI†) following a literature procedure,[27,28] and their reactions with Cu(II) salts systematically investigated. Reaction of $Cu(ClO_4)_2·6H_2O$ with H_3L^1 in MeOH in the presence of NaOH provided [Na{Cu_2(μ-OH)(μ-L^1)}$_2$]ClO_4 (**1**, Scheme 1). Use of NEt_3 in MeOH or the absence of NaOH did not provide the H_2O bridged [Cu_2] complex. The complex precipitated directly from the reaction mixture as a green solid in ~75% yield. The preparation of complex **1** is summarized in eqn (1), accounting for the trapping of Na^+ from the added NaOH during synthesis.

$$2H_3L^1 + 4Cu(ClO_4)_2 \cdot 6H_2O + 8NaOH \rightarrow [Na\{Cu_2(\mu\text{-}OH)(\mu\text{-}L^1)\}_2]ClO_4 + 7NaClO_4 + 30H_2O \quad (1)$$

The microanalytical and solution electrical conductivity data in DMF are consistent with the formula [Na{Cu_2(μ-L^1)-(μ-OH)}$_2$]ClO_4 for **1**. However no sign of formation of neutral hydroxido-bridged species [Cu_2(μ-OH)(μ-L^1)] was observed, perhaps because of the higher solubility of monocationic **1**, which crystallizes with a central Na^+ ion to assemble a pair of neutral [Cu_2(μ-OH)(μ-L^1)] units around it (*vide supra*). To establish the role of steric crowding on the ligand backbone for crown-ether like coordination of two tris-phenolate fragments around Na^+, a reaction has been carried out with H_3L^2 under similar reaction conditions. The green complex [Cu_2(μ-OH)-(μ-L^2)](**2**) (Scheme 1) was directly synthesized in ~75% yield in MeOH medium under aerobic conditions at room temperature by stirring a reaction mixture of $Cu(ClO_4)_2·6H_2O$, H_3L^2 and NaOH in 2 : 1 : 4 molar ratio for 1 h. The synthesis of **2** from H_3L^2 is summarized in eqn (2).

$$H_3L^2 + 2Cu(ClO_4)_2 \cdot 6H_2O + 4NaOH \xrightarrow{2\,MeOH} [Cu_2(\mu\text{-}OH)(\mu\text{-}L^2)] + 4NaClO_4 + 15H_2O \quad (2)$$

The microanalytical and solution electrical conductivity data confirm the dinuclear entity for **2**.

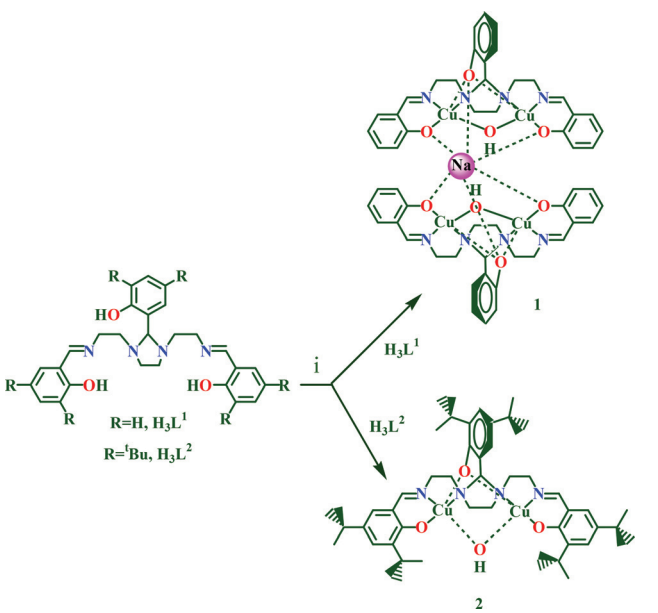

Scheme 1 Reaction of $Cu(ClO_4)_2·6H_2O$ with H_3L^1 and H_3L^2 in MeOH in the presence of NaOH: *Reagents and conditions*: i $2H_3L^n$ + $4Cu(ClO_4)_2·6H_2O$ + 8NaOH in MeOH, room temp.

Description of structures

Single crystals suitable for X-ray structure determination were obtained by slow evaporation of saturated CH_3CN and MeOH solutions of **1** and **2** after 6 days and one week, respectively. The crystallographic data are summarized in Table 1 and selected bond lengths and bond angles are collected in Table 2.

[Na{Cu_2(μ-OH)(μ-L^1)}$_2$]ClO_4 (1). The molecular structure of **1** is shown in Fig. 1, and important bond lengths and bond angles are given in Table 2. Compound **1** crystallizes from a MeCN solution in the trigonal $R\bar{3}$ space group. The double asymmetric unit contains one tetranuclear complex and one perchlorate anion. The absence of [Cu_2(μ-OH)(μ-L^1)] as an independent dinuclear species suggests that the assembled heteropentametallic [$NaCu_4$] species is stable as a discrete molecule in the solid state. The tetranuclear complex consists of two deprotonated $[L^1]^{3-}$ ligands, each of them delivering a set of N_4O_3 donor atoms to the [Cu_4] complex that assembles around a central Na^+ ion located on a centre of symmetry. Electroneutrality of the complex is ensured by one uncoordinated ClO_4^- anion available from the metal salt. Two hydroxido groups complete the coordination environments around each Cu(II) site (Fig. 1 and 2). The Na^+ ion at the center of the complex is surrounded by four Cu(II) ions organized in a

Table 1 Crystallographic data for **1** and **2**

Compound	**1**	**2**
Formula	$C_{54}H_{56}N_8O_8Cu_4{\cdot}Na^+{\cdot}ClO_4^-$	$C_{51}H_{76}N_4O_4Cu_2{\cdot}1.5H_2O$
M_r/g mol^{-1}	1321.67	1093.41
Space group	$R\bar{3}$	$C2/c$
Crystal system	Trigonal	Monoclinic
a/Å	35.6139(6)	23.2607(12)
b/Å	35.6139(6)	19.7554(10)
c/Å	11.4732(1)	28.1663(14)
α/°	90.0	90.0
β/°	90.0	101.913(2)
γ/°	120	90.0
V/Å^3	12 602.4(3)	12 664.3(11)
T/K	295	295
Z	9	8
D_c/g cm^{-3}	1.567	1.010
F(000)	6084	4120
μ(Mo-Kα)/cm^{-1}	16.22	7.11
R_{int}	0.0328	0.0804
Obsd reflns $[I \geq 2\sigma(I)]$	5018	6417
$R(F^2)$ (obsd reflns)	0.0427	0.0664
w$R(F^2)$ (all reflns)	0.1356	0.2023
No. of variables	379	561
GOF	1.047	0.992
$\Delta\rho_{max,min}$/e Å^{-3}	0.798; −0.614	0.628; −0.367
CCDC No.	651162	840821

rectangular geometry with short and long Cu···Cu distances at 3.018 and 6.088 Å and the longest diagonal Cu···Cu distance is 6.789 Å (Fig. S1, ESI†). Two Cu(II) ions are held together by one fully deprotonated heptadentate $[L^1]^{3-}$ ligand through bridging central imidazolidine and phenoxido moieties and one exogenous μ-HO^- group derived from H_2O of solvent media.

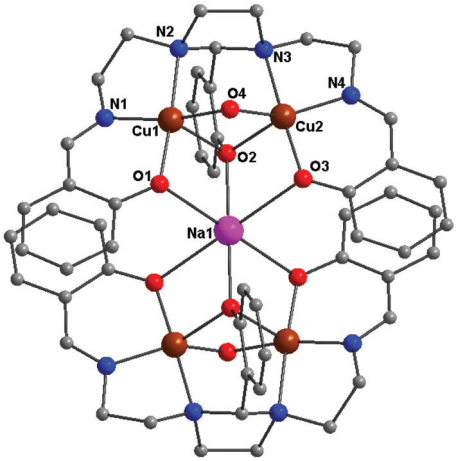

Fig. 1 View of the cationic $[Na\{Cu_2(\mu\text{-}OH)(\mu\text{-}L^1)\}_2]^+$ unit in **1** with atom-numbering scheme. H atoms are omitted for clarity. Color code: Cu brown, N blue, O red, C gray.

The N_3O_2 coordination environments around the Cu(II) ions are between square-pyramidal (*sp*) and trigonal-bipyramidal (*tbp*) (τ is 0.187 and 0.617 for Cu1 and Cu2, respectively).[26] The only clearly identifiable *apical* position of Cu1 is occupied by O2 (Cu1–O2, 2.364 Å), the central bridging phenoxido oxygen atom (μ-O_{Ph}) of the ligand, which takes, by contrast, a *basal* position of Cu2 (*apical–basal* bridging, *a,b*; Cu2–O2, 2.163 Å). In turn, the bridging hydroxide oxygen atom (μ-O_{hyd}) binds to the short *basal* position of Cu2 (at 61.7% *tbp* geometry) (Cu2–O4, 2.028 Å) and also uses a shorter *basal* site of Cu1 (*basal–basal*, *b,b*; Cu1–O4, 1.919 Å) (Chart 2). Complexes featuring a $[Cu_2(\mu\text{-}O_{Ph})(\mu\text{-}O_{hyd})]$ moiety having a (*a,b* + *b,b*)

Table 2 Selected interatomic distances (Å) and angles (°) for **1** and **2**

1				**2**			
Cu1–N1	1.921(3)	Cu2–O3	1.919(2)	Cu1–O4	1.958(3)	Cu1–O2	2.196(3)
Cu1–O4	1.919(2)	Cu2–N4	1.940(3)	Cu2–O4	1.942(3)	Cu2–O2	1.906(3)
Cu1–O1	1.935(2)	Cu2–O4	2.028(2)	Cu1–O1	1.909(3)	Cu2–N4	1.933(4)
Cu1–N2	2.130(3)	Cu2–N3	2.085(3)	Cu1–N1	1.924(4)	Cu2–O3	2.094(3)
Cu1–O2	2.364(2)	Cu2–O2	2.163(2)	Cu1–N2	2.131(3)	Cu2–N3	2.291(4)
Cu1–Na1	3.4003(3)	Cu2–Na1	3.3945(4)	Cu1–Cu2	3.0150(8)		
Cu1–Cu2	3.0184(5)	Na1–O1	2.619(2)				
Na1–O2	2.315(2)	Na1–O3	2.601(2)				
N1–Cu1–O4	165.7(1)	O3–Cu2–N4	94.4(1)	O1–Cu1–O3	102.1(1)	O3–Cu2–O2	130.7(1)
N1–Cu1–O1	92.8(1)	O3–Cu2–O4	89.6(1)	O1–Cu1–O4	90.2(1)	O2–Cu2–O4	91.0(1)
O4–Cu1–O1	91.7(1)	N4–Cu2–O4	139.9(1)	O1–Cu1–N1	91.9(1)	O2–Cu2–N3	144.7(2)
N1–Cu1–N2	84.1(1)	O3–Cu2–N3	176.8(1)	O1–Cu1–N2	168.6(1)	O2–Cu2–N4	91.0(2)
O4–Cu1–N2	91.1(1)	N4–Cu2–N3	83.6(1)	O3–Cu1–O4	81.5(1)	O3–Cu2–O4	84.6(1)
O1–Cu1–N2	176.9(1)	O4–Cu2–N3	93.5(1)	O3–Cu1–N1	105.8(1)	O3–Cu2–N3	84.6(1)
N1–Cu1–O2	108.7(1)	O3–Cu2–O2	91.0(1)	O3–Cu1–N2	89.3(1)	O3–Cu2–N4	99.9(1)
O4–Cu1–O2	84.6(1)	O4–Cu2–O2	87.6(1)	O4–Cu1–N1	171.8(2)	O4–Cu2–N3	92.3(1)
O1–Cu1–O2	92.3(1)	N4–Cu2–O2	132.1(1)	O4–Cu2–N2	92.3(1)	O4–Cu2–N4	172.0(2)
N2–Cu1–O2	89.1(1)	N3–Cu2–O2	88.7(1)	N1–Cu1–N2	84.1(2)	N3–Cu2–N4	81.6(2)
N1–Cu1–Na1	111.90(8)	O3–Cu2–Na1	49.61(7)	Cu1–O3–Cu2	89.3(1)	Cu1–O4–Cu2	101.3(1)
O4–Cu1–Na1	81.27(7)	N4–Cu2–Na1	130.83(9)				
O1–Cu1–Na1	50.08(6)	O4–Cu2–Na1	80.08(7)				
N2–Cu1–Na1	131.65(7)	N3–Cu2–Na1	130.50(8)				
O2–Cu1–Na1	42.83(5)	O2–Cu2–Na1	42.42(5)				
Cu1–O2–Cu2	83.51(7)	Cu1–O4–Cu2	99.73(10)				

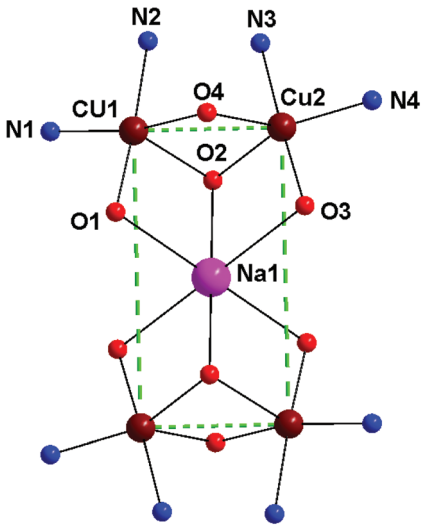

Fig. 2 View of the atom connectivity within the [$NaCu_4$] rectangular core with the phenoxido and hydroxido bridges in **1**. Each phenoxido bridge (O2) joins the *apical* position of one copper (Cu1) atom with the *basal* position of the other (Cu2). Color code: Cu brown, N blue, O red.

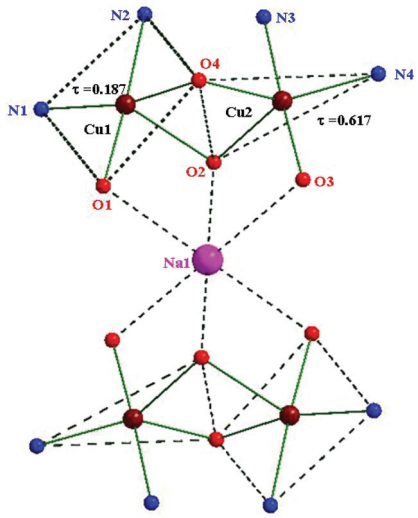

Chart 2

distribution are not very common in the literature of copper complexes. Important parameters are the Cu–O_{Ph}–Cu and Cu–O_{hyd}–Cu angles, which are 83.5 and 99.7°, respectively. Twisting of the imidazolidine ring containing chelating arms makes the ligand flexible which in turn supports asymmetrical coordination environments around two copper(II) ions within the binuclear unit. C8–C9–N2–C12 (imidazolidine) and C20–C19–N3–C12 (imidazolidine) torsion angles on either side of the ring are 90.02 and 173.15°, respectively, for the *basal–apical* phenolate bridge. The particular arrangement of the ligand around the two Cu(II) ions results in the formation of a [–O–Cu–O–Cu–O–] moiety properly disposed to provide two O_3 *facial* units for a distorted octahedral

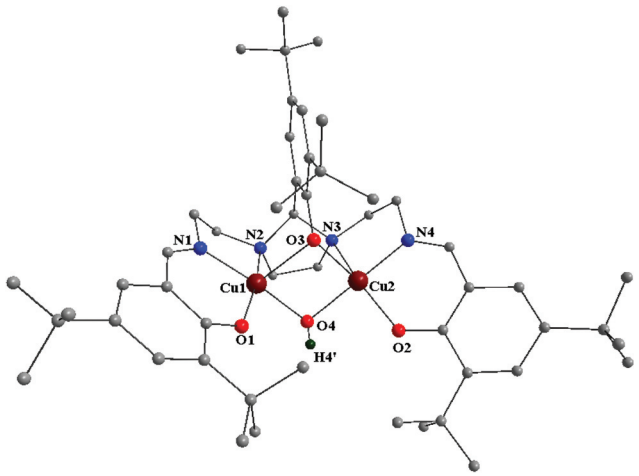

Fig. 3 Molecular view of the neutral dinuclear [$Cu_2(\mu\text{-}L^2)(\mu\text{-}OH)$] unit in **2** with atom-numbering scheme. H atoms are omitted for clarity. Color code: Cu brown, N blue, O red, C gray.

coordination environment around the central Na^+ cation, responsible for the stability of the [$NaCu_4$] assembly. The distances of six oxygen atoms from Na1 fall within the interval observed on other metallacrowns or metallacryptates.[46–48] The tetranuclear [$Cu_2L^1(OH)$]···Na^+···[$Cu_2L^1(OH)$] assembly is further held together by means of π–π interactions established between terminal phenyl rings of the two ligands where the distances between the calculated centroids of the interacting phenyl rings are 3.596 Å (Fig. S2 in the ESI†). The face-to-face orientation of the O donors of each ligand in [$Cu_2L^1(OH)$] in staggered form is responsible for the generation of the cavity during packing in which the Na^+ ion fits nicely (Fig. S3†). The uncoordinated perchlorate anion is disordered. The particular face-to-face orientation of the [Cu_2] units along with perchlorate anions is responsible for the existence of cavities.

[$Cu_2(\mu\text{-}L^2)(\mu\text{-}OH)$]·1.5$H_2O$ (2). A green block-like single crystal obtained by slow evaporation of a MeOH solution of complex **2** was used to determine the molecular structure by X-ray crystallography. It crystallizes in the monoclinic *C*2/*c* space group. The molecular structure of **2** is depicted in Fig. 3, and the relevant metric parameters are collected in Table 2. The asymmetric part of the unit cell contains one neutral [$Cu_2(L^2)(OH)$] unit, a water molecule in general position and a water molecule in special position on a twofold axis. The $[L^2]^{3-}$ ligand in **2** is arranged as in **1**, providing N_2O_2 donor sets around the copper atoms that include a μ-phenoxido bridge originating from its central pendant arm bound to the imidazolidine ring. A single hydroxido group occupies the fifth coordination site around each Cu(II) (Fig. 3).

The hydroxide bridge gives an intradimer Cu···Cu distance of 3.015 Å that is similar to the shortest intradimer Cu···Cu distance found in **1**. The pentacoordinated N_3O_2 coordination environments around the Cu(II) ions are between square-pyramidal (*sp*) and trigonal-bipyramidal (*tbp*) (τ is 0.060 and 0.470 for Cu1 and Cu2, respectively).[26] The Cu–O distances in the bridging region indicate that the oxido bridge is practically

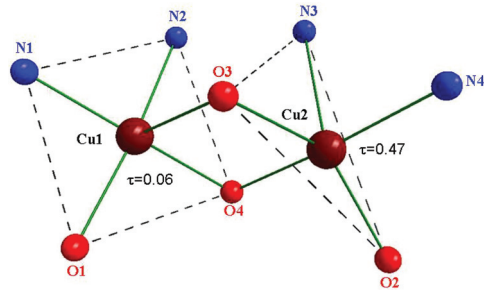

Chart 3

symmetrical (Cu1–O4 = 1.958 Å; Cu2–O4 = 1.942 Å) whereas the phenoxido bridge is particularly unsymmetrical (2.196 and 2.094 Å). Therefore, the $[Cu_2(\mu\text{-}O_{Ph})(\mu\text{-}O_{hyd})]$ moiety has a similar (*a,b* + *b,b*) distribution to that found in **1**. This phenoxido bridge may be considered as an *apical–basal* one with respect to a *sp–tbp* (47% *tbp* geometry) $[Cu_2]$ complex (Chart 3). Important parameters are the Cu–O_{Ph}–Cu and Cu–O_{hyd}–Cu angle, which are 89.3 and 101.3°, respectively. Two tridentate ONO halves of the ligand binds differently with Cu1 and Cu2 making N–Cu–O angles of 168.6 and 144.7°. The particular arrangement of the ligand around the two Cu(II) ions results in a [–O–Cu–O–Cu–O–] arrangement which is entirely different from that obtained in case of complex **1**. Instead of a O_3 *facial* arrangement these O atoms (O1, O2 and O4) remain in an angular orientation not suitable for coordination of Na^+ in a metallacrown like assembly. The tertiary amine nitrogen atoms of the imidazolidine ring form longer Cu–N bonds of 2.131 and 2.291 Å, respectively. The $[Cu_2O_2]$ diamond stacks over the imidazolidine pentagon at 2.657 Å. The presence of seven water solvates and one methanol molecule within the crystal lattice demonstrate the role of these molecules for crystallization. No compound with higher nuclearity is seen with these molecules. The space-filling models indicates the distribution of water molecules at the surface of the Cu_2 dinuclear complex (Fig. S4, ESI†).

IR spectroscopy

The characteristic bands of the $[L^1]^{3-}$ and $[L^2]^{3-}$ ligands appear clearly on the FT-IR spectra of the two complexes. The $\tilde{\nu}_{C=N}$ stretching bands are observed at 1624 and 1638 cm^{-1} for **1** and **2**. Moreover, strong and broad absorption bands are observed at 3435 and 3314 cm^{-1} due to the $\tilde{\nu}_{OH}$ stretching mode of the HO^- bridging groups.[49] As expected, this band is missing in the spectra of the free ligands. The strong single band for $\tilde{\nu}_{ClO_4}$ at around 1108 cm^{-1} for **1** suggest the presence of uncoordinated perchlorate anions.[50]

Electronic spectra

The complexes in CH_3CN solutions show multiple bands in the 200–900 nm region. The ligand-field spectra of the complexes show broad absorption bands (λ), with maxima at 600 nm (ε = 406 L mol^{-1} cm^{-1}) and 668 nm (ε = 152 L mol^{-1} cm^{-1}) for **1** and **2**, respectively. The intense absorptions below 400 nm at 269 nm (ε = 15 990 L mol^{-1} cm^{-1}) and 253 nm (ε = 21 000 L mol^{-1} cm^{-1}) are dominated by the metal ion bound ligand-based absorptions for **1** and **2**, respectively. Spectra of these complexes also show shoulders at 370 nm (ε = 5560 L mol^{-1} cm^{-1}) and 392 nm (ε = 4640 L mol^{-1} cm^{-1}) respectively, due to HO^- → Cu(II) and/or PhO^- → Cu(II) ligand-to-metal charge transfer (LMCT) transitions.[14]

Magnetic properties

The solid-state magnetic properties of **1** and **2** have been investigated by dc susceptibility measurements down to 1.8 K at 0.1 T (Fig. 4). For **1**, the χT product at room temperature is 1.6 cm^3 K mol^{-1}, that is slightly higher than the theoretical value of 1.5 cm^3 K mol^{-1} (with g = 2) expected for four isolated paramagnetic Cu^{II} ions (d^9, S = 1/2). Upon cooling, the χT product first increases to reach a value of 1.81 cm^3 K mol^{-1} at 16 K, and then decreases to reach a value of 1.53 cm^3 K mol^{-1} at 2 K. This indicates that dominant ferromagnetic interactions occur between Cu^{II} ions in the compound. The low-temperature behavior is the result of weaker intra-molecular antiferromagnetic exchange interactions between the paramagnetic centers. For **2**, the χT product at room temperature is 0.84 cm^3 K mol^{-1}, that is slightly higher than the theoretical value of 0.75 cm^3 K mol^{-1} (with g = 2) expected for two isolated paramagnetic Cu^{II} ions (d^9, S = 1/2). Upon cooling, the χT product is first stable then starts to decrease slightly below 20 K to reach the value of 0.78 cm^3 K mol^{-1} at 2 K. This behavior indicates weak antiferromagnetic interactions between the Cu(II) ions.

Keeping in mind the structure of **1**, the magnetic pathways are expected to be more efficient in the double oxido-

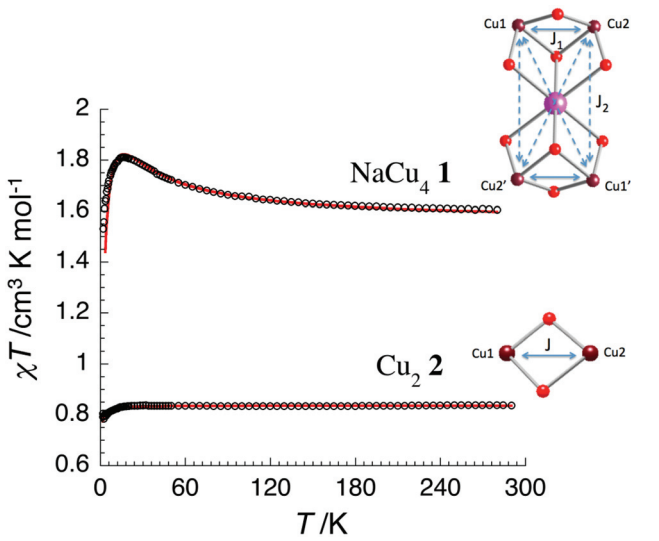

Fig. 4 Temperature dependence of the χT products for **1** and **2** at 1000 Oe (with χ defined as molar magnetic susceptibility equal to M/H per mole of complex). The red solid lines are the best fits of the experimental data using tetramer and dimer spin models (see main text), respectively.

phenoxido bridged [Cu_2] units compared to the ones existing through the Na bridge. Therefore, **1** can be described as a rectangle with two exchange constants, J_1 in the double oxido-phenoxido bridged [Cu_2] pairs and J_2 through the Na bridge in all the other Cu(II) pairs, as shown in Fig. 4. The following Heisenberg isotropic spin Hamiltonian has been used to describe the exchange interactions in **1**:

$$H = -2J_1(S_{Cu1} \cdot S_{Cu2} + S_{Cu1'} \cdot S_{Cu2'}) - 2J_2((S_{Cu1} + S_{Cu2}) \cdot (S_{Cu1'} + S_{Cu2'})) \quad (3)$$

The application of the van Vleck equation[51] allows the determination of the low-field analytical expression of the magnetic susceptibility:[52]

$$\chi T = \frac{2N\mu_B^2 g_{Cu}^2}{k_B} \frac{2\exp(2J_1/k_BT) + \exp((4J_1 - 2J_2)/k_BT) + 5\exp((4J_1 + 2J_2)/k_BT)}{1 + 6\exp(2J_1/k_BT) + \exp((4J_1 - 4J_2)/k_BT) + 3\exp((4J_1 - 2J_2)/k_BT) + 5\exp((4J_1 + 2J_2)/k_BT)} \quad (4)$$

This model is able to reproduce the experimental data of **1** with the following parameters g_{Cu} = 2.05(3), J_1/k_B = +12.9(2) K and J_2/k_B = −1.0(2) K. The positive sign of J_1 implies that the two oxido-phenoxido Cu dinuclear units in **1** possess an S_T = 1 spin ground state whereas the other magnetic interactions between the Cu(II) ions are antiferromagnetic and weak considering the negative and small J_2 value.

To reproduce the experimental magnetic data in **2**, a simple dinuclear S = 1/2 spin model has been applied with the following Heisenberg isotropic spin Hamiltonian (eqn. (5)) giving the analytical expression of the magnetic susceptibility (eqn (6)):

$$H = -2J(S_{Cu1} \cdot S_{Cu2}) \quad (5)$$

$$\chi T = \frac{2N\mu_B^2 g_{Cu}^2}{k_B} \frac{1}{3 + \exp(-2J/k_BT)} \quad (6)$$

The best fit of the χT *vs.* T for **2** and the best set of parameters obtained using eqn (5) and (6) are g_{Cu} = 2.11(1), J/k_B = −0.25(1) K. The negative sign of the J parameter implies that the Cu dinuclear unit in **2** possesses an S_T = 0 spin ground state.

The difference in the exchange couplings found in the oxido-phenoxido bridged [Cu_2] pairs, J_1 and J for **1** and **2**, respectively, can be explained by structural differences in the [$Cu_2(\mu\text{-}O_{Ph})(\mu\text{-}O_{hyd})$] moiety. Generally speaking for the Cu^{II} ions, the magnetic interactions mediated through their *apical* positions are much weaker than those mediated by bridges coordinated on the *basal* sites. Therefore, if one considers only the magnetic pathways that involve equatorial bonds around each Cu^{II} ions, the complexes **1** and **2** may be viewed as two almost isolated Cu1–Cu2 dinuclear units with a *single* hydroxido bridge with Cu–O_{hyd}–Cu angles of 99.7 and 101.3°, respectively. Therefore, the change from ferromagnetic to antiferromagnetic coupling between **1** and **2** is related to the opening of the Cu–O_{hyd}–Cu angle favoring the orbital overlap between the Cu(II) ions, as is well-known in the hydroxido Cu(II) dinuclear core.[53] More surprising are the antiferromagnetic interactions observed in **1** at low temperature which are found to be larger in intensity than the antiferromagnetic interactions found in **2**, as observed with the bigger J_2 absolute value compared to J. For **1**, they are attributed to exchange interactions through the Na bridge despite the long distances between the Cu(II) ions (between 6 and 7 Å). Nevertheless, it is worth noting that these J_2 interactions are certainly overestimated by our model, as their estimations also contain the effects of the intermolecular interactions.

Interaction of complex 1 with DNA

The binding characteristics of the cationic complex **1** with DNA have been examined by electronic absorption spectroscopy. The neutral complex **2** has not been studied. The binding to DNA leads to marked changes in the electronic spectra of this type of complexes,[54] as the complex/DNA assembly *via* covalent and/or non-covalent interactions[55,56] is expected to perturb the ligand based electronic transitions of the complexes. Both 'hyperchromism' and 'hypochromism' can be observed, where the former suggests the rupture of the secondary structure of DNA, while the latter is characteristic of complex intercalation[57] attributed to the interaction between the electronic states of the chromophore in the complex and those of the DNA bases,[58] while the red shift is associated with the decrease in the energy gap between the highest occupied and the lowest unoccupied molecular orbitals (HOMO and LUMO) after binding of the complex to DNA.[59] The existence of a red-shift is also indicative of the stabilization of the DNA duplex.[54] The absorption spectra of **1** in the presence and in the absence of CT DNA (at a constant concentration of complexes, 0.16×10^{-4} M) are shown in Fig. 5. Complex **1** displays bands at 269 and 362 nm, corresponding to the π–π* transition and LMCT bands, respectively. Upon increasing the concentration of CT DNA, a concomitant increase in absorption intensities is observed with hyperchromism of 55–60% in the intraligand region and of 20–22% in the LMCT region with a significant red shift of 2–4 nm. The hyperchromism along with substantial red shift for compound **1** unambiguously revealed the active participation of aromatic chromophores *via* partial intercalation, in addition to favorable electrostatic interaction of the cationic core to the polyanionic phosphate backbone of the DNA double helix.[60] These changes in spectra can be ascribed to strong binding interaction leading to the alteration in the conformation of DNA.[61,62] Furthermore, the spectral features are also evocative of an end-stacking binding mode and could involve supplementary interactions with DNA loops and phosphate backbone. To evaluate quantitatively, the binding strength of compound **1** with CT DNA, the intrinsic binding constant, K_b, was determined with eqn (7) by monitoring the changes in absorbance of the π–π* bands with increasing concentration of CT DNA, where [DNA] represents the

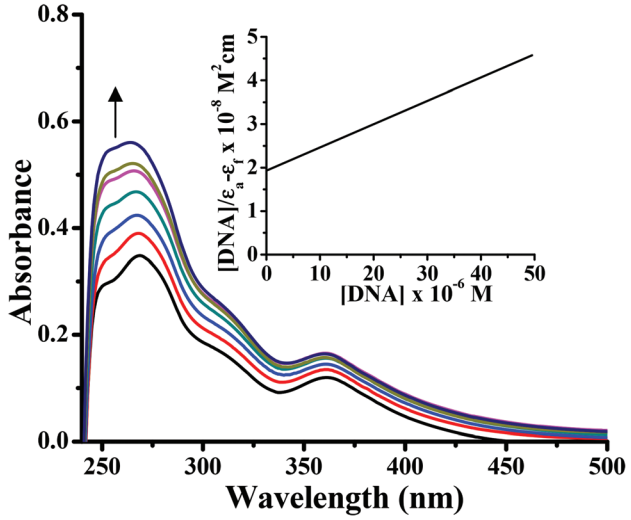

Fig. 5 Absorption spectra of **1** in a 5% DMF–5 mM Tris-HCl–50 mM NaCl buffer at pH 7.2 in the absence (R = 0) and presence of (R = 25) of increasing amounts of CT DNA.

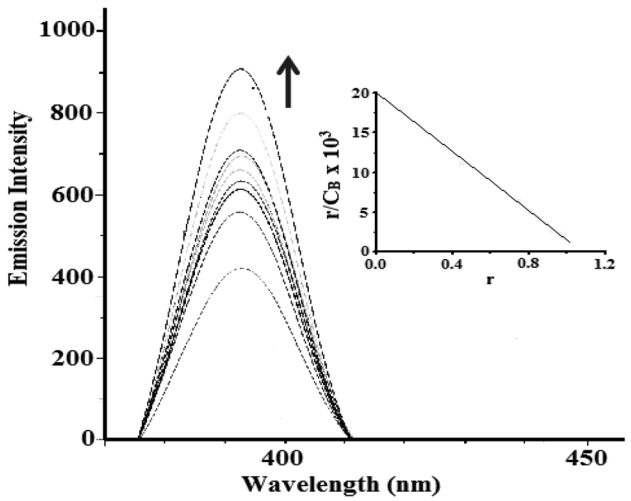

Fig. 6 Emission spectra of **1** in DMF, in the absence and in presence of CT DNA in 5 mM Tris-HCl–50 mM NaCl, pH = 7.2, at room temperature.

concentration of DNA, ε_a, ε_f and ε_b are the apparent extinction coefficients A_{obs}/[complex], the extinction coefficient for free metal complex and the extinction coefficient for metal complex in the fully bound form, respectively.

$$[DNA]/|\varepsilon_a - \varepsilon_f| = [DNA]/|\varepsilon_b - \varepsilon_f| + 1/K_b|\varepsilon_b - \varepsilon_f| \quad (7)$$

In the plots of $[DNA]/\varepsilon_a - \varepsilon_f$ *vs.* [DNA], K_b is given by the ratio of the slope to the intercept. The intrinsic binding constant of **1** was found to be 0.9×10^4 M^{-1}.

Complex **1** is luminescent in DMF and Tris-HCl buffer around 395–398 nm at room temperature, when excited at 364 and 391 nm, respectively. The luminescence spectra of **1** in the absence and presence of CT DNA are depicted in Fig. 6. Upon subsequent addition of CT DNA (0 to 0.33×10^{-4} M), there was significant enhancement in the fluorescence intensity without apparent change in the shape and position of the emission bands. Although the emission enhancement cannot be regarded as a criterion for binding mode, it is related to the extent to which the complex gets into the hydrophobic environment inside the DNA and reduces the accessibility of solvent molecules to complex. Hydrophobic interactions between the complexes and polyelectrolyte may induce changes in the excited state properties either due to electrostatic association or partial intercalation.[63]

Furthermore, the cationic complexes usually bind to DNA non-covalently as the cationic core of the complexes exerts a strong electrostatic attraction to the anionic phosphate backbone of DNA, thus precluding substantial overlap with the base pairs leading to higher emission intensity indicative of electrostatic binding to the DNA. It is interesting to note that an increase in emission intensity yields the electrostatic association. The intercalative mode of binding depends upon the ligand characteristics such as (1) planarity of ligand, (2) extent of aromatic π-system available for stacking, and (3) depth of ligand which can penetrate into the double helix. On the other hand, electrostatic interaction would be more sensitive to the charge of the metal ion, ligand hydrophobicity, and size of the complex.[64] The CT DNA binding constant of the complex **1** was obtained as $K = 1.02 \times 10^4$ M^{-1} with a mean standard deviation of ±0.05.

In order to examine the ability of the compound to displace 3,8-diamino-5-ethyl-6-phenylphenanthridinium bromide (EB) from the EB–DNA complex, a competitive EB binding study has been undertaken with fluorescence experiments.[65,66] EB is a phenanthridine fluorescence dye and is known as a typical indicator of intercalation.[67] It can form soluble complexes with nucleic acids emitting intense fluorescence in the presence of CT DNA due to the intercalation of the planar phenanthridinium ring between adjacent base pairs on the double helix.[68] The changes observed in the spectra of EB on its binding to CT DNA are used for the interaction study between DNA and metal complexes.[69]

Upon the addition of **1** (0–40 μM) to CT DNA pretreated with EB ([EB]/[DNA] = 0.1) in a 5% DMF–5 mM Tris-HCl–50 mM NaCl buffer at pH 7.1, the emission intensity of DNA-bound EB decreases. The emission intensity in the absence and presence of both the complexes with EB-DNA are depicted in Fig. 7. As there is significant quenching of the EB-induced emission intensity, thus the partial intercalative mode for the complexes cannot be ruled out. The Stern–Volmer constant K_{SV} is often used to evaluate the quenching efficiency for each complex and varies with the experimental conditions, where, I_o and I are the emission intensities in the absence and presence of the complex, respectively.

$$I_o/I = 1 + K_{SV}[complex] \quad (8)$$

The K_{SV} value for complex **1** was found to be 1.4×10^4 M^{-1}.

Change in the electrophoretic mobility of plasmid DNA on agarose gel is commonly taken as an evidence for direct DNA–

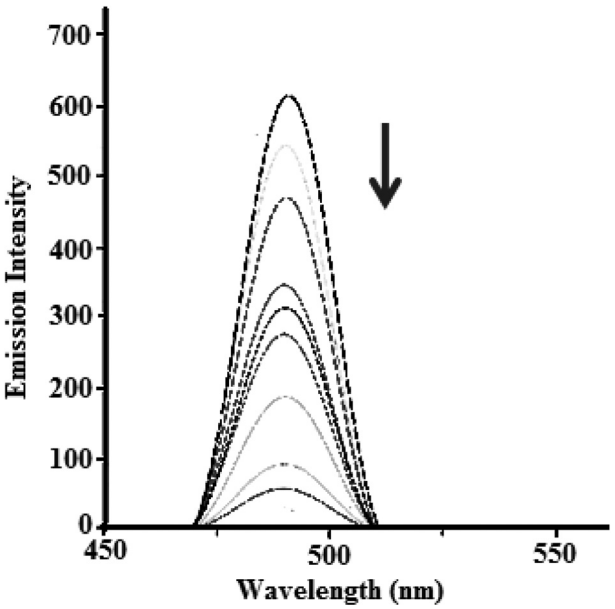

Fig. 7 Emission quenching spectra of **1** with increasing concentration of quencher EB in the absence and presence of CT DNA in Tris-HCl buffer at pH 7.2 at room temperature. Arrow shows the intensity changes with the increasing concentration of EB.

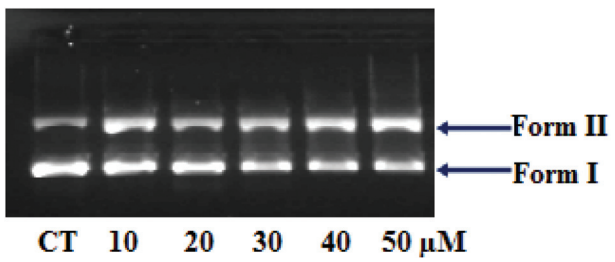

Fig. 8 The cleavage pattern of the agarose gel electrophoresis for pBR322 DNA (300 ng) by **1** (10–50 μM) after 1 h incubation time (concentration-dependent).

metal interactions. Alteration of the DNA structure causes retardation in the migration of supercoiled DNA and a slight increase in the mobility of open circular DNA to a point where both forms comigrate. The DNA cleaving ability of complexes was demonstrated initially by a plasmid relaxation assay, in which the conversion of super-coiled form (Form I, SC) to nicked circular (Form II, NC) or linear open circular (Form III, LC) DNA were monitored. A concentration-dependent DNA cleavage by compound **1** was performed in which supercoiled pBR322 DNA (300 ng) was incubated with increasing concentration in 5% DMF–5 mM Tris-HCl–50 mM NaCl buffer at pH 7.2 for 1 h and then subjected to gel electrophoresis. The electrophoretic pattern observed for compound **1** with the increase in concentration of the complex (10–50 μM), indicates plasmid DNA was converted from Form I to Form II, while no conversion to Form III was observed. The amounts of Form I DNA decreased whereas those of Form II increased to more than 80% at a concentration of 50 μM (Fig. 8).

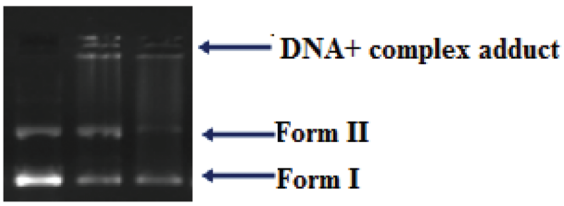

Fig. 9 Agarose gel electrophoresis pattern for the cleavage of pBR322 DNA (300 ng) by **1** in the presence of DNA minor groove binding agent DAPI and major groove binding agent methyl green at room temperature after incubation for 30 min.

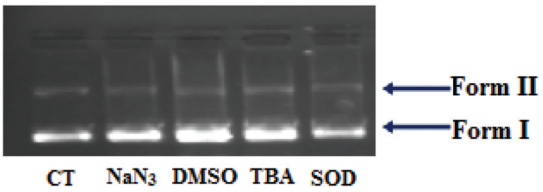

Fig. 10 Agarose gel electrophoresis pattern for the cleavage of pBR322 DNA (300 ng) by **1** in the presence of standard radical scavengers at room temperature after incubation for 30 min.

DNA recognition elements (groove binding) minor groove binding agent, DAPI and major groove binding agent, methyl green[70,71] were used to probe the potential interacting site of compound **1** with supercoiled pBR322 DNA. The supercoiled pBR322 DNA was treated with DAPI or methyl green prior to the addition of complex. The patterns presented in Fig. 9 demonstrated that **1** shows preferential selectivity towards the major groove of the DNA helix.

The comparative cleavage reactions were carried out to predict the cleavage mechanism of pBR322 plasmid DNA by **1** in the presence of various radical scavengers (Fig. 10) such as DMSO, *tert*-butyl alcohol as OH^- radical scavenger,[72] NaN_3 as $^1O_2$ scavenger,[73] and superoxide dismutase (SOD) as superoxide anion radical ($O_2^{\cdot -}$) scavenger.[65] The cleavage pattern observed showed significant inhibition of cleavage in all the cases *viz.* NaN_3, DMSO, TBA, SOD with complex **1**.

X-Ray crystallography

The crystal parameters and other experimental details of the data collection for **1** and **2** are summarized in Table 1. In each case, a crystal of suitable size was selected from the mother-liquor and mounted on the tip of a glass fiber and cemented using epoxy resin. Single-crystal data of complex **1** were collected on a Nonius Kappa CCD diffractometer using graphite-monochromated Mo-Kα radiation (λ = 0.7107 Å) at 295 K. Data sets were integrated with the Denzo SMN package[74] and corrected for Lorentz-polarization and absorption[75] effects. The structure was solved by direct methods (SIR97)[76] and refined by full-matrix least-squares methods with all non-hydrogen atoms anisotropic and hydrogens included on calculated positions, riding on their carrier atoms. The H4 hydrogen of the hydroxo group was located on a difference Fourier map and

refined isotropically. The ClO_4^- anion was found disordered and was refined with occupancy of 0.5. Each oxygen was refined isotropically over two sites. All calculations were performed using SHELXL-97[77] in the WINGX system of programs.[78] Single-crystal data of the complex **2** were collected on a Bruker APEX II CCD X-ray diffractometer using graphite-monochromated Mo-Kα radiation (λ = 0.7107 Å). Data were collected at 295 K. The refinement was performed using full-matrix least squares with non-hydrogen atoms refined anisotropically, except the methylic groups belonging to three disordered *tert*-butyl groups which were refined isotropically over two sites. To increase stability of refinement, a system of restraints to the *tert*-butyl geometries was employed. The hydrogen atoms were geometrically fixed on calculated positions, riding on their carrier atoms. The H4 hydrogen of the hydroxo group was located on a difference Fourier map and refined isotropically. During the refinement it was possible to localize and refine only two water molecules, one in general position and the latter on a special position on a twofold axis. However, because the presence of an ill-defined region of residual density, the refinement was far from satisfactory. For this reason the program SQUEEZE was used to cancel out the effects of the disordered solvent. SQUEEZE is part of the PLATON program system[79] and attempts to remove mathematically the effects of disordered solvent.

The graphics were generated using Diamond 3.1e software.

Conclusions

Homotetranuclear copper complexes have become a promising class of coordination cage in which variation of the metal salt, ligands or experimental conditions lead to a variety of structural motifs showing characteristic magnetic and biological properties. In this work use of an imidazolidine-based unsubstituted tris-phenolate ligand leads to a Na^+ mediated assembly of two neutral $[Cu_2L^1]$ complex fragments in **1**. The di-*tert*-butyl group substituted analogue H_3L^2, on the other hand confirms the independent existence of the neutral $[Cu_2(OH)(L^2)]$ components in complex **2**, indicating the role of steric-crowding on the ligand part for Na^+ templated self-aggregation reaction. Complex **1** showed ferromagnetic interactions in the double oxido-phenoxido $[Cu_2]$ moiety and complex **2** showed weak antiferromagnetic interactions within the same fragment. These results demonstrate the templating role of the Na^+ cation that changes the geometry of the hydroxido bridges. Complex **1** in solution showed evidences of binding to CT DNA as investigated through a variety of techniques and registered efficient cleavage by oxidative mechanism supported by ROS quenching experiments. Formation of other self-assembled coordination cages with other cationic species and bridging groups is under investigation.

Acknowledgements

A. S. is thankful to the University Grant Commission, New Delhi, India for the research fellowship. The authors also thanks DST, New Delhi, for providing the Single Crystal X-ray Diffractometer facility in the Department of Chemistry, IIT Kharagpur under its FIST program. V. B. acknowledges the Italian Ministry of University and Scientific Research, MIUR, Rome, Italy. R. C. and C. M. acknowledge the University of Bordeaux, Région Aquitaine, GIS Advanced Materials in Aquitaine (COMET Project), the Institut Universitaire de France (IUF) and the CNRS for financial support. We are thankful the reviewers for their constructive suggestions which have improved the quality of the present paper.

Notes and references

1 C. J. Pedersen, *J. Am. Chem. Soc.*, 1970, **92**, 391.
2 D. Mandal, V. Bertolasi, G. Aromí and D. Ray, *Dalton Trans.*, 2007, 1989.
3 L. Y. Wang, S. Igarashi, Y. Yukawa, Y. Hoshino, O. Roubeau, G. Aromí and R. E. P. Winpenny, *Dalton Trans.*, 2003, 2318.
4 A. Caneschi, A. Cornia and S. J. Lippard, *Angew. Chem., Int. Ed. Engl.*, 1995, **34**, 467.
5 R. W. Saalfrank, I. Bernt, E. Uller and F. Hampel, *Angew. Chem., Int. Ed. Engl.*, 1997, **36**, 2482.
6 Y. Yukawa, G. Aromí, S. Igarashi, J. Ribas, S. A. Zvyagin and J. Krzystek, *Angew. Chem., Int. Ed.*, 2005, **44**, 1997.
7 A. R. Paital, C. S. Hong, H. C. Kim and D. Ray, *Eur. J. Inorg. Chem.*, 2007, 1644.
8 P. K. Nanda, G. Aromí and D. Ray, *Chem. Commun.*, 2006, 3181.
9 M. Sarkar, R. Clérac, C. Mathonière, N. G. R. Hearns, V. Bertolasi and D. Ray, *Inorg. Chem.*, 2010, **49**, 6575.
10 M. Bera, W. T. Wong, G. Aromí, J. Ribas and D. Ray, *Inorg. Chem.*, 2004, **43**, 4787.
11 A. R. Paital, D. Mandal, X. Huang, J. Li, G. Aromí and D. Ray, *Dalton Trans.*, 2009, 1352.
12 A. R. Paital, A.-Q. Wu, G.-C. Guo, G. Aromí, J. Ribas-Ariño and D. Ray, *Inorg. Chem.*, 2007, **46**, 2947.
13 A. Banerjee, S. Sarkar, D. Chopra, E. Colacio and K. K. Rajak, *Inorg. Chem.*, 2008, **47**, 4023.
14 A. R. Paital, T. Mitra, D. Ray, W. T. Wong, J. Ribas-Ariño, J. J. Novoa, J. Ribasa and G. Aromí, *Chem. Commun.*, 2005, 5172.
15 D. Lahiri, T. Bhowmick, B. Pathak, O. Shameema, A. K. Patra, S. Ramakumar and A. R. Chakravarty, *Inorg. Chem.*, 2009, **48**, 339.
16 P. K. Nanda, V. Bertolasi, G. Aromí and D. Ray, *Polyhedron*, 2009, **28**, 987.
17 K. S. Banu, T. Chattopadhyay, A. Banerjee, S. Bhattacharya, E. Suresh, M. Nethaji, E. Zangrando and D. Das, *Inorg. Chem.*, 2008, **47**, 7083.
18 S. Striegler, M. Dittel, R. Kanso, N. A. Alonso and E. C. Duin, *Inorg. Chem.*, 2011, **50**, 8869.
19 A. R. Paital, V. Bertolasi, G. Aromí, J. Ribas-Ariño and D. Ray, *Dalton Trans.*, 2008, 861.

20 A. R. Paital, C. S. Hong, H. C. Kim and D. Ray, *Eur. J. Inorg. Chem.*, 2007, 1644.
21 A. R. Paital, P. K. Nanda, S. Das, G. Aromí and D. Ray, *Inorg. Chem.*, 2006, **45**, 505.
22 P. K. Nanda, G. Aromí and D. Ray, *Inorg. Chem.*, 2006, **45**, 3143.
23 M. Bera, W. T. Wong, G. Aromi, J. Ribas and D. Ray, *Inorg. Chem.*, 2004, **43**, 4787.
24 M. Sarkar, R. Clérac, C. Mathonière, N. G. R. Hearns, V. Bertolasi and D. Ray, *Inorg. Chem.*, 2011, **50**, 3922.
25 A. K. Ghosh and D. Ray, *Polyhedron*, 2013, **52**, 370.
26 E. Wong, S. Liu, T. Liigger, F. E. Hahn and C. Orvig, *Inorg. Chem.*, 1995, **34**, 93.
27 P. Wei and D. Atwood, *Chem. Commun.*, 1997, 1427.
28 P. M. May and D. R. Williams, in *Metal Ions in Biological Systems*, ed. H. Sigel, Marcel Dekker, New York, 1981, vol. 12, ch. 7.
29 *Metal Ions in Biological Systems*, ed. H. Sigel, Marcel Dekker, New York, 1981, vol. 13.
30 T. Miura, A. Hori-i, H. Mototani and H. Takeuchi, *Biochemistry*, 1999, **38**, 11560.
31 B. C. Bales, T. Kodama, Y. N. Weledji, M. Pitie, B. Meunier and M. M. Greenberg, *Nucleic Acids Res.*, 2005, **33**, 5371.
32 P. Uma Maheswari, S. Roy, H. D. Dulk, S. Barends, G. V. Wezel, B. Kozlevcar, P. Gamez and J. Reedijk, *J. Am. Chem. Soc.*, 2006, **128**, 710.
33 J. D. Ranford, P. J. Sadler and D. A. Tocher, *J. Chem. Soc., Dalton Trans.*, 1993, 3393.
34 C. H. Ng, K. C. Kong, S. T. Von, P. Balraj, P. Jensen, E. Thirthagiri, H. Hamada and M. Chikira, *Dalton Trans.*, 2008, 447.
35 S. Ramakrishnan, D. Shakthipriya, E. Suresh, V. S. Periasamy, M. A. Akbarsha and M. Palaniandavar, *Inorg. Chem.*, 2011, **50**, 6458.
36 K. J. Humphreys, K. D. Karlin and S. E. Rokita, *J. Am. Chem. Soc.*, 2002, **124**, 6009.
37 L. Li, K. D. Karlin and S. E. Rokita, *J. Am. Chem. Soc.*, 2005, **127**, 520.
38 (*a*) K. J. Humphreys, K. D. Karlin and S. E. Rokita, *J. Am. Chem. Soc.*, 2001, **123**, 5588; (*b*) K. J. Humphreys, K. D. Karlin and S. E. Rokita, *J. Am. Chem. Soc.*, 2002, **124**, 8055.
39 K. J. Humpreys, A. J. Hohnson, K. D. Karlin and S. E. Rokita, *JBIC, J. Biol. Inorg. Chem.*, 2002, **7**, 835.
40 L. Li, K. D. Karlin and S. E. Rokita, *J. Am. Chem. Soc.*, 2005, **127**, 520.
41 J. Marmur, *J. Mol. Biol.*, 1961, **3**, 208.
42 M. E. Reichmann, S. A. Rice, C. A. Thomas and P. Doty, *J. Am. Chem. Soc.*, 1954, **76**, 3047.
43 A. Wolfe, G. H. Shimmer and T. Meehan, *Biochemistry*, 1987, **26**, 6392.
44 F. Arjmand, K. Banerjee and M. Chauhan, *Inorg. Chem.*, 2007, **46**, 3072.
45 D. Mandal, M. Chauhan, F. Arjmand, G. Aromí and D. Ray, *Dalton Trans.*, 2009, 9183.
46 L. Y. Wang, S. Igarashi, Y. Yukawa, Y. Hoshino, O. Roubeau, G. Aromı and R. E. P. Winpenny, *Dalton Trans.*, 2003, 2318.
47 J. Ribas, A. Escuer, M. Monfort, R. Vicente, R. Cortes, L. Lezama and T. Rojo, *Coord. Chem. Rev.*, 1999, **193–195**, 1027.
48 G. L. Zhuang, W. X. Chen, H. X. Zhao, X. J. Kong, L. S. Long, R. B. Huang and L. S. Zheng, *Inorg. Chem.*, 2011, **50**, 3843.
49 K. Motoda, H. Sakiyama, N. Matsumoto, H. Okawa and D. E. Fenton, *J. Chem. Soc., Dalton Trans.*, 1995, 3419.
50 (*a*) D. L. Lewis, W. E. Hatfield and D. J. Hodgson, *Inorg. Chem.*, 1974, **13**, 147; (*b*) J. Foley, D. Kennefick, D. Phelan, S. Tyagi and B. J. Hathaway, *J. Chem. Soc., Dalton Trans.*, 1983, 2333.
51 J. H. van Vleck, *The Theory of Electric and Magnetic Susceptibility*, Oxford University Press, 1932.
52 (*a*) B. Abarca, R. Ballesteros, M. Chadlaoui, C. Ramirez de Arellano and J. A. Real, *Eur. J. Inorg. Chem.*, 2007, 4574; (*b*) A. Burkhardt, E. T. Spielberg, H. Gorls and W. Plass, *Inorg. Chem.*, 2008, **47**, 2485.
53 (*a*) D. J. P. Hodgson, *Inorg. Chem.*, 1975, **19**, 173; (*b*) V. H. Crawford, H. W. Richardson, J. R. Wasson, D. J. Hodgson and W. E. Hatfield, *Inorg. Chem.*, 1976, **15**, 2107.
54 T. M. Kelly, A. B. Tossi, D. J. McConnell and T. C. Strekas, *Nucleic Acids Res.*, 1985, **13**, 6017.
55 Q. L. Zhang, J. G. Liu, H. Chao, G. Q. Xue and L. N. Ji, *J. Inorg. Biochem.*, 2001, **83**, 49.
56 A. Tarushi, G. Psomas, C. P. Raptopoulou and D. P. Kessissoglou, *J. Inorg. Biochem.*, 2009, **103**, 898.
57 T. Afrati, A. A. Pantazaki, C. Dendrinou-Samara, C. Raptopoulou, A. Terzis and D. P. Kessissoglou, *Dalton Trans.*, 2010, **39**, 765.
58 B. D. Wang, Z. Y. Yang, P. Crewdson and D. Q. Wang, *J. Inorg. Biochem.*, 2007, **101**, 1492.
59 J. H. Tan, Y. Lu, Z. S. Huang, L. Q. Gu and J. Y. Wu, *Eur. J. Inorg. Chem.*, 2007, **42**, 1169.
60 (*a*) M. Baldini, M. B. Ferrari, F. Bisceglie, G. Pelosi, S. Pinelli and P. Tarasconi, *Inorg. Chem.*, 2003, **42**, 2049; (*b*) A. K. Patra, S. Dhar, M. Nethaji and A. R. Chakrvarty, *Dalton Trans.*, 2005, 896.
61 A. M. Pyle, J. P. Rehmann, R. Meshoyrer, C. V. Kumar, N. J. Turro and J. K. Barton, *J. Am. Chem. Soc.*, 1989, **111**, 3053.
62 Y. M. Song, Q. Yang, P. J. Wu, N. N. Luan, L. F. Wang and Y. M. Liu, *J. Inorg. Biochem.*, 2006, **100**, 1685.
63 B. L. Hauenstein, W. J. Dressick, S. L. Buell, J. N. Demas and B. A. De-Graff, *J. Am. Chem. Soc.*, 1983, **105**, 4251.
64 C. V. Kumar, J. K. Barton and N. J. Turro, *J. Am. Chem. Soc.*, 1985, **107**, 5518.
65 A. Dimitrakopoulou, C. Dendrinou-Samara, A. A. Pantazaki, M. Alexiou, E. Nordlander and D. P. Kessissoglou, *J. Inorg. Biochem.*, 2008, **102**, 618.
66 K. Jiao, Q. X. Wang, W. Sun and F. F. Jian, *J. Inorg. Biochem.*, 2005, **99**, 1369.

67 W. D. Wilson, L. Ratmeyer, M. Zhao, L. Strekowski and D. Boykin, *Biochemistry*, 1993, **32**, 4098.
68 C. G. Reihardt and T. R. Krugh, *Biochemistry*, 1978, **17**, 4845.
69 G. H. Zhao, H. K. Lin, S. R. Zhu, H. W. Sun and Y. T. Chen, *J. Inorg. Biochem.*, 1998, **70**, 219.
70 E. Trotta, N. Del Grosso, M. Erba and M. Paci, *Biochemistry*, 2000, **39**, 6799.
71 B. Selvakumar, V. Rajendiran, U. Maheswari, H. Stoeckli-Evans and M. Palaniandavar, *J. Inorg. Biochem.*, 2006, **100**, 316.
72 M. S. Melvin, M. W. Calcutt, R. E. Noftle and R. A. Manderville, *Chem. Res. Toxicol.*, 2002, **15**, 742.
73 C. J. Burrows and J. G. Muller, *Chem. Rev.*, 1998, **98**, 1109.
74 Z. Otwinowski and Z. Minor, in *Methods Enzymol*, ed. C. W. Carter and R. M. Sweet, Academic Press, London, 1977, vol. 276, Part A, p. 307.
75 R. H. Blessing, *Acta Crystallogr., Sect. A: Found. Crystallogr.*, 1995, **51**, 33.
76 A. Altomare, M. C. Burla, M. Camalli, G. L. Cascarano, C. Giacovazzo, A. Moliterni, A. G. G. Polidori and R. Spagna, *J. Appl. Crystallogr.*, 1999, **32**, 115.
77 G. M. Sheldrick, *SHELXL97, Program for Crystal Structure Refinement*, University of Göttingen, Göttingen, Germany, 1997.
78 L. Farrugia, *J. Appl. Crystallogr.*, 1999, **32**, 837.
79 A. L. Spek, *Acta Crystallogr., Sect. D: Biol. Crystallogr.*, 2009, **65**, 148.

